DOI: 10.1002/chem.200601225

Structural and Dynamic Characterization of Copper(II) Binding of the Human Prion Protein Outside the Octarepeat Region

Francesco Berti,[c] Elena Gaggelli,[b] Remo Guerrini,[d] Anna Janicka,[a] Henryk Kozlowski,*[a] Anna Legowska,[e] Hanna Miecznikowska,[e] Caterina Migliorini,[b] Rebecca Pogni,[b] Maurizio Remelli,[f] Krzysztof Rolka,[e] Daniela Valensin,[b] and Gianni Valensin*[b]

Abstract: Human prion protein (hPrP) fragments encompassing the 91–120 region, namely hPrP92–100 (SP1), hPrP106–113 (SP2), hPrP91–120 (LP1), and hPrP91–114 (LP2), were considered for delineation of the Cu^{II}-binding site(s). NMR and EPR spectroscopy results obtained from LP1 or LP2 were compared with those obtained from SP1 and SP2. The coexistence of two binding sites, one centered at His96 and the other at His111, was evidenced and ratified by ESI mass spectrometry at low and high metal:peptide ratios. While room-temperature NMR spectroscopy data were consistent with the binding site centered on His111 being approximately fourfold stronger than that centered on His96, low-temperature EPR spectroscopy results yielded evidence for the opposite trend. This disagreement, which has also occurred in the literature, was clarified by temperature-dependent molecular dynamics runs that demonstrated Met112 approaching the metal at room temperature, a process that is expected to stabilize the His111-centered binding site through hydrophobic shielding of the metal coordination sphere.

Keywords: binding studies · coordination modes · copper · peptides · prion proteins

Introduction

The prion protein, PrP^C, is generally agreed to normally play a functional role in copper transport, sequestration, or antioxidant activity.[1] PrP^C may undergo a conformational transformation to a protease-resistant isoform, known as PrP^{Sc}, which is prone to aggregation. PrP^{Sc} is the putative infectious agent of transmissible spongiform encephalopathies (TSE) or prion diseases.[2] These diseases have been linked to an imbalance of metal homeostasis in the brain and hypotheses have been made for an association with the loss of copper binding from PrP^C on conversion into PrP^{Sc}.[3,4] The two prion isoforms are identical in primary structure, but they differ in secondary-structure elements[5] and possess considerably different physicochemical properties.[6–10] PrP^C is a proteinase-K-sensitive α-helical monomer,[11–14] while PrP^{Sc} is an assembled multimer that is resistant to proteinase digestion and has an increased amount of β structure.[15]

The ability of the prion protein to bind Cu^{II} in vitro, as well as in vivo, is well documented and widely suggested to play a relevant role in copper homeostasis or in copper-based enzymatic activity.[16–21]

[a] Dr. A. Janicka, Prof. H. Kozlowski
Faculty of Chemistry, University of Wroclaw
F. Joliot-Curie 14, 50383 Wroclaw (Poland)
Fax: (+48) 71-375-7251
E-mail: henrykoz@wchuwr.chem.uni.wroc.pl.

[b] Prof. E. Gaggelli, Dr. C. Migliorini, Prof. R. Pogni, Dr. D. Valensin, Prof. G. Valensin
Department of Chemistry, University of Siena
via Aldo Moro, 53100 Siena (Italy)
Fax: (+39) 0577-234-231
E-mail: valensin@unisi.it.

[c] Dr. F. Berti
Novartis Vaccines, 53100 Siena (Italy)

[d] Dr. R. Guerrini
Department of Pharmaceutical Sciences
University of Ferrara, Ferrara (Italy)

[e] Dr. A. Legowska, Dr. H. Miecznikowska, Prof. K. Rolka
Faculty of Chemistry, University of Gdansk, Gdansk (Poland)

[f] Prof. M. Remelli
Department of Chemistry, University of Ferrara, Ferrara (Italy)

Supporting information for this article is available on the WWW under http://www.chemeurj.org/ or from the author.

Initial studies focusing on the octarepeat region (ORR) of the protein of human origin (hPrP60–91) suggested that there might be as many as four cooperative Cu^{II}-binding sites on PrP^{C}.[22–25] The direct link between copper and prion disease was challenged by the observation that transgenic mice expressing a truncated version of PrP with the ORR removed are still susceptible to prion infection.[26] However, studies of different PrP fragments have suggested that the protein could strongly bind a fifth Cu^{II} atom outside the ORR[16,18,27] and that the affinity of this site towards Cu^{II} may increase upon ORR deletion.[28] The location of this fifth site and the exact structure of bound Cu^{II} is still a matter of debate. Three sites, each associated with a histidine residue, namely His96,[16,21] His111,[29] and a His residue in the C-terminal globular domain,[30] have been suggested. The occurrence of a Cu^{II}-binding site within the unstructured region between the N-terminal domain and the structured C-terminal domain is potentially relevant in the light of the role suggested for this region in amyloid formation and infectivity in TSE.[31–35] The need for delineation of Cu^{II}-binding equilibria within this region is further ratified by the recent observations that 1) Cu^{II} catalyzes proteolytic cleavage of PrP^{C} before residue 90, instead of the normal breakdown at around residue 111, and 2) the generated 19 kDa PrP fragment may seed the polymerization of wild-type PrP^{C}.[36] While Cu^{II} binding in the repeat region is reasonably well characterized, different and often conflicting conclusions have been obtained from studies on the residues offering Cu^{II}-binding site(s) in the human PrP92–126 fragment:

1. EPR spectroscopy suggests His96 to be the unique locus for metal coordination.[37]
2. EXAFS data indicate His111, Met112, and His96 to be binding residues.[38]
3. CD spectroscopy suggests the binding of Cu^{II} to His96 and His111 simultaneously or independently from each other.[39,40]
4. Potentiometric and spectroscopic studies on Cu^{II} fragments containing His111 have been performed and revealed the existence of 3N[41] or 3N1S[42] complexes that are dominant at physiological pH values.

Herein, potentiometric and spectroscopic features of Cu^{II} complexes with hPrP fragments encompassing the 91–120 region at pH 6.5 have been used to delineate the Cu^{II}-binding sites located in this region. A diverse affinity of these sites was demonstrated by comparison with shorter hPrP fragments comprising either His96 or His111 as Cu^{II}-anchoring sites. The considered short fragments, hPrP92–100 and hPrP106–113, have already been reported to represent the minimal binding motif able to coordinate the metal.[40] The paramagnetic effects of Cu^{II} upon the NMR parameters have been particularly considered in obtaining geometrical restraints in molecular dynamics simulations that yield the 3D solution structures of the metal complexes.

Results

Potentiometric titrations: The protonation constants of monoprotic hPrP92–100 (short peptide 1, SP1) are reported in Table 1S in the Supporting Information; those of hPrP106–113 (short peptide 2, SP2) have been reported elsewhere.[41] Copper succeeds in displacing protons from both peptides from approximately pH 4. This yields diversely protonated complex species depending on the pH value, as shown by species-distribution diagrams (Figure 1S in the Supporting Information). The species which forms at the lowest pH value is CuL, with the His imidazole moiety as the unique binding group (L = ligand). Two amide protons are then displaced from the complex in a quick sequence, to form the $CuH_{-2}L$ complex, which dominates at physiological pH values. In the alkaline pH range, this complex undergoes two additional deprotonation steps, therby leading to the formation of $CuH_{-3}L$ (from a third amide nitrogen atom) and $CuH_{-4}L$ (most likely from a metal-bound second imidazole nitrogen atom).

The hPrP91–120 (long peptide 1, LP1) and hPrP91–114 (long peptide 2, LP2) peptides behave as H_7L acids, the protonation constants of which are summarized in Tables 2S and 3S in the Supporting Information. Potentiometric titrations yield evidence for the formation of nine Cu^{II} species (Figure 2S and Figure 3S in the Supporting Information). Within the physiological pH range, the CuH_2L and CuHL complexes dominate.

UV/Vis and CD parameters: CD spectra of Cu^{II}–SP1 and Cu^{II}–SP2[41] show some typical absorptions: 1) a d–d double band in the visible region, 2) a negative band at around 310 nm, due to a charge-transfer transition from a deprotonated amido nitrogen atom to the copper atom, 3) a positive band located at 250–260 nm, attributable to a $\pi 2$ imidazole to copper transition, and 4) a positive band at around 330 nm, attributable to a $\pi 1$ imidazole to copper transition.

The UV/Vis absorption spectra are characterized by a large band which becomes more and more intense at rising pH values; at the same time, its maximum undergoes a regular blue shift. The wavelength of maximum absorption is close to 800 nm at the most acidic pH values, as expected for the Cu^{II} hexa-aquo complex; it reaches 550 nm in alkaline solution, a value compatible with a square planar or tetragonally distorted octahedral complex with four nitrogen donors coordinated in the plane and a possible additional interaction in the axial position.

The CD spectra of Cu^{II}–LP1 and Cu^{II}–LP2 suggest an $\{N_{imid},2N^{-}\}$ donor set in CuH_2L (d–d bands at 605 and 522 nm) and an additional amide coordination in CuHL species (bands at 580 and 511 nm) which results in an $\{N_{imid},3N^{-}\}$ coordination mode.[43,44] The data for Cu^{II}–LP1 and for Cu^{II}–LP2 are similar to each other, with the longer peptide forming species that are distinctly more stable, most likely due to protection of the metal-ion-binding site by the hydrophobic tail.

NMR measurements: The NMR experiments on Cu^{II}–SP1 were exclusively performed at pH 6.5 where the 3N $CuH_{-2}L$ complex dominates. Upon copper addition, a selective and conspicuous broadening was observed for His proton resonances (Figure 4S in the Supporting Information), where the aromatic His signals have completely vanished in the presence of the paramagnetic ion. ^{1}H–^{13}C HSQC alpha cross-peaks affected during Cu^{II} titration were identified by comparing their intensities (I) with those of the same cross-peaks (I_0) observed in the absence of the paramagnetic ion. The largest broadening was monitored for the His96 correlation (Figure 1 A), which completely disappears in the presence of 0.1 Cu^{II} equivalents. Among the other correlations, the most affected are the ones belonging to Thr95, Ser97, and Gln98 at all of the metal concentrations used. Figure 1 A additionally shows that an increase in copper concentration determines larger broadening of all cross-peaks, with a conserved trend during the metal titration, which suggests a preserved copper coordination whatever the metal:ligand ratio.

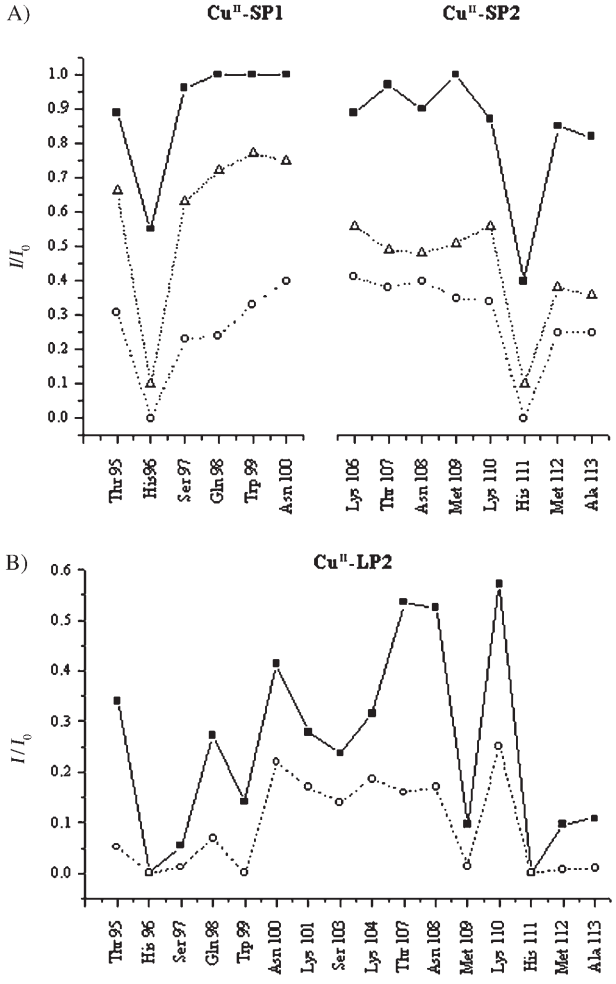

Figure 1. I/I_0 profiles of the ^{1}H–^{13}C HSQC NMR signals of: A left) 4.5 mM SP1 at pH 6.5 in the presence of 0.02 (■), 0.05 (△), and 0.1 (○) Cu^{II} equivalents; A right) 4.5 mM SP2 at pH 6.5 in the presence of 0.1 (■), 0.2 (▲), and 0.4 (○) Cu^{II} equivalents; B) 4.5 mM LP2 at pH 6.5 in the presence of 0.1 (■) and 0.4 (○) Cu^{II} equivalents.

The paramagnetic relaxation rate contributions, R_{1p}, of several protons are shown in Table 1. Excluding His96 protons, the most affected nuclei are the Gly93, Gly94, Thr95, Ser97, and Gln98 Hα protons, which exhibit similar values of R_{1p}, in the range of 2.70–2.90 s^{-1}. These concomitant effects on residues either preceding or following His96 suggest that two different binding modes are allowed, with Cu^{II} deprotonating and binding either the His96 and Thr95 or Ser97 and Gln98 amide nitrogen atoms.

When adding Cu^{II} to SP2 at pH 6.5 (Figure 5S in the Supporting Information), the His aromatic protons are the first to be affected, as is usual for Cu^{II} anchoring at the imidazole ring.[45,46] In the same way as with SP1, the ^{1}H–^{13}C HSQC experiments allowed the detection of the most affected alpha correlations (Figure 1 A). Involvement of His111 in metal binding was confirmed, as its correlation was completely washed out by 0.4 Cu^{II} equivalents. In addition, the decrease in the intensity of the Met112 and Ala113 cross-peaks, at all of the investigated metal concentrations, suggests the proximity of these residues to the metal center.

Broadening of ^{13}C resonances was also analyzed, which revealed that the Met112 and Ala113 Cα (Figure 2 A) and His111 and Met112 carbonyl atoms (Figure 2 B) are the most affected ones; these results strongly indicate the involvement of the Met112 and Ala113 amide nitrogen atoms in metal binding. Furthermore, the absence of any detectable effects on the Met109 and Met112 methyl carbon atoms (Figure 2 C) excludes any direct metal binding to the sulfur atoms.

The paramagnetic contributions measured on SP2 protons (Table 1) confirm that the Met112 and Ala113 amide nitrogen atoms belong to the Cu^{II} coordination sphere, because the corresponding Hα R_{1p} values are the largest ones.

NMR spectra of LP1 were measured at pH 6.5 in order to gain information about the dominant 3N CuH_2L complexes. Similar results were obtained with LP2, thus supporting the view that the hydrophobic hPrP115–120 tail is not involved in the direct metal-ion coordination.[39,45] The addition of copper caused selective proton line broadening on His aromatic and β protons (Figure 6S in the Supporting Information). The exclusive disappearance of both the His96 and His111 signals implies their involvement in the metal-ion binding, consistent with the initial anchoring of Cu^{II} by the imidazole nitrogen atoms.

The ^{1}H-^{13}C HSQC results, shown in Figure 1 B, reveal the most affected regions in LP2 (and LP1) to be located in the immediate neighborhood of the two His residues: the alpha correlations of His96 and His111 completely disappear in the presence of 0.1 Cu^{II} equivalents, while those of Ser97, Trp99, Met109, Met112, and Ala113 are almost washed out after the addition of 0.4 metal equivalents. The conserved paramagnetic effects at both copper concentrations indicate the formation of a unique metal-coordination pathway, even in the presence of small amounts of the paramagnetic ion.

The paramagnetic enhancements of proton spin-lattice relaxation rates, R_{1p} (Figure 3 A), disclose that, besides the extremely broadened His96 and His111 signals, the most af-

Table 1. Paramagnetic relaxation rate contributions, R_{1p} and calculated Cu^{II}–H distances for 4.5 mM SP1 and SP2 in the presence of 0.1 and 0.2 Cu^{II} equivalents, respectively, at pH 6.5 and $T=298$ K.

	SP1				SP2		
	H	R_{1p} [s^{-1}]	r [nm]		H	R_{1p} [s^{-1}]	r [nm]
Gly92	α	1.78	0.68±0.01	Lys106	α	0.83	0.99±0.005
					γ	0.86	0.99±0.005
					ε	1.13	0.92±0.005
Gly93	α	2.79	0.32±0.08[a]	Thr107	α	0.80	1.00±0.005
					β	0.90	0.98±0.005
					γ	1.11	0.93±0.005
Gly94	α	2.75	0.32±0.08[a]	Asn108	α	1.31	0.89±0.005
					β	1.22	0.91±0.005
Thr95	α	2.85	0.32±0.08[a]	Met109[b]/	α	2.25	
	γ	2.11	0.62±0.02	Met112[b]	β	2.47	
					γ	2.32	
					ε	1.75	
Ser97	α	2.70	0.32±0.08[a]	Lys110	α	1.87	0.79±0.005
	β	2.11	0.62±0.02		γ	1.15	0.92±0.005
					ε	2.94	0.54±0.001
Gln98	α	2.72	0.32±0.08[a]	Ala113	α	3.14	0.32±0.08[a]
	β	2.03	0.63±0.02		β	2.15	0.74±0.005
	γ	1.81	0.67±0.01				
Trp99	α	1.44	0.73±0.005				
	δ1	2.20	0.60±0.02				
	ζ2	2.21	0.60±0.02				
Asn100	α	0.75	0.88±0.005				
	β	0.35	1.03±0.005				

[a] Imposed for k_{off} calculation (see the text for details). [b] Met109 and Met112 were not unequivocally assigned.

fected protons belong to Thr95, Ser97, Gln98, Met109, Lys110, Met112, and Ala113. When these values are compared with those reported in Table 1, an almost identical trend can be observed, which apparently suggests that the two distinct copper-binding regions, one located at His96 and the other at His111, are preserved in LP1. This behavior is reminiscent of a reported CD study,[40] where the CD spectrum of the Cu^{II} complex with hPrP91–115 was observed to formally arise from a linear combination of the separate CD spectra of the Cu^{II} complexes with the His96→Ala hPrP91–115 and His111→Ala hPrP91–115 PrP analogues, each containing a single Cu^{II} site.

Direct involvement of the methionine sulfur in Cu^{II} binding was excluded by 1) the absence of large paramagnetic effects on the methyl groups of either Met109 or Met112 and 2) the effectiveness of copper binding in peptide fragments where nLeu is substitute for Met (Figure 3B). Some indirect effect derived from the methionine residue can, however, be observed as the Met→nLeu substitution results in a homogeneous distribution of meaningful R_{1p} values between the two His regions (Figure 3B), while larger effects are monitored in the proximity of His111, rather than around His96, in the original peptide.

EPR measurements: EPR spectroscopy of Cu^{II} complexes with the investigated peptides was performed on samples containing 0.4 equivalents of Cu^{II}, conditions similar to those of the NMR experiments. The 120 K EPR spectra of the Cu^{II} complex with LP1 (Figure 4A) can be simulated by linearly combining the EPR spectra of the two Cu^{II}–SP1 and Cu^{II}–SP2 complexes at the same temperature. These EPR spectra (Figure 4B and C) could be simulated by considering Cu^{II} bound by three nitrogen atoms in nearly tetragonal sites (Table 2). In agreement with Cu^{II} bound by N_{imid} and $2N^-$ donors,[37,39–41] analysis of the section of the Fourier Transform (FT) sensitive to the nitrogen-number parity of the experimental EPR spectrum and the corresponding section of the FT of the simulated spectrum[47] ratifies the occurrence of an odd number of nitrogen atoms in the coordination sphere. Furthermore, the $g_{\|}$ and $A_{\|}$ values for the Cu^{II}–SP1 and Cu^{II}–SP2 complexes are in the range of equatorial coordination of three nitrogen ligands and one oxygen ligand (3N,1O) according to the Peisach–Blumberg plot.[48] The possibility of equatorial coordination of a sulfur ligand from Met109 or Met112, in the case of Cu^{II}–SP2, can be ruled out. The EPR spectrum of the complex gives a $g_{\|}$ value of >2.2, which excludes the presence of a sulfur atom in the first coordination sphere of the copper.

ESI-MS measurements: The ESI mass spectra, acquired in positive-ion mode at an LP2:Cu^{II} ratio of 1:0.4 (Figure 5), show that the signal of the free peptide at m/z 663.0 is accompanied by a new peak at m/z 679.0, accounted for by a 1:1 association, such that NMR data, obtained at the same concentration ratios, can be suitably interpreted in terms of 1:1 complexes only. The coexistence of the two Cu^{II}-binding sites is further supported by ESI mass spectra recorded at higher concentrations of Cu^{II}, that is, at an LP2:Cu^{II} ratio of 1:1.25. Together with the already mentioned peaks, a new peak at m/z 694 becomes detectable, thereby providing evidence for a complex where two Cu^{II} ions are bound by the same peptide molecule.

Discussion

The potentiometric and spectroscopic results for Cu^{II}–SP1, Cu^{II}–SP2, and Cu^{II}–LP2 indicate that the complex having the metal bound to the His imidazole and two amide nitrogen atoms is the main species in the pH range 6.2–7.5, with the highest predominance at pH 6.5–6.8. pH 6.5 was therefore selected for NMR experiments.

The measured paramagnetic relaxation rates allow the calculation of the Cu^{II}–proton distances to be used in molec-

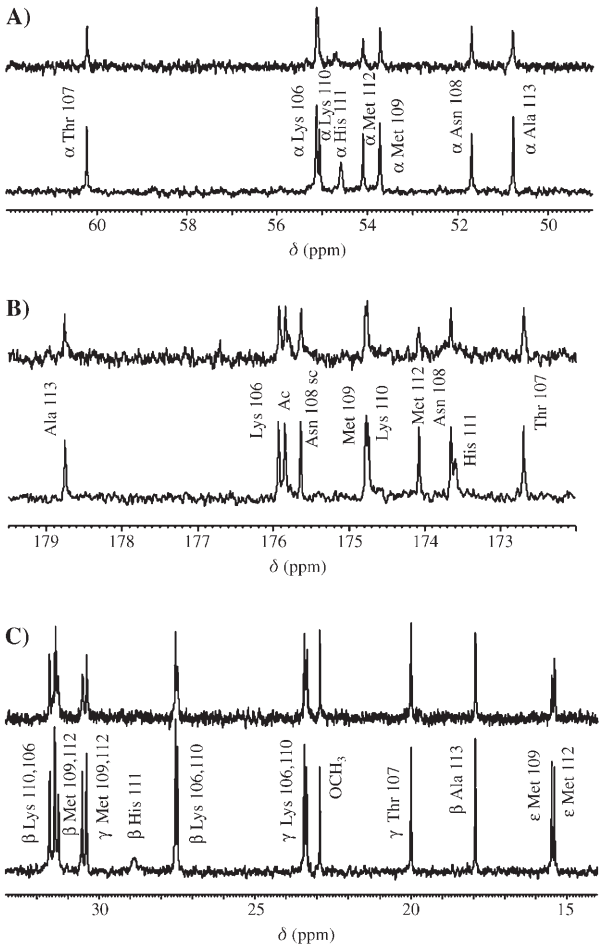

Figure 2. ^{13}C NMR spectra of 4.5 mM SP2 at pH 6.5 and $T=298$ K before (lower trace) and after (upper trace) the addition of 0.2 Cu^{II} equivalents. A) α region; B) carbonyl region; C) aliphatic region.

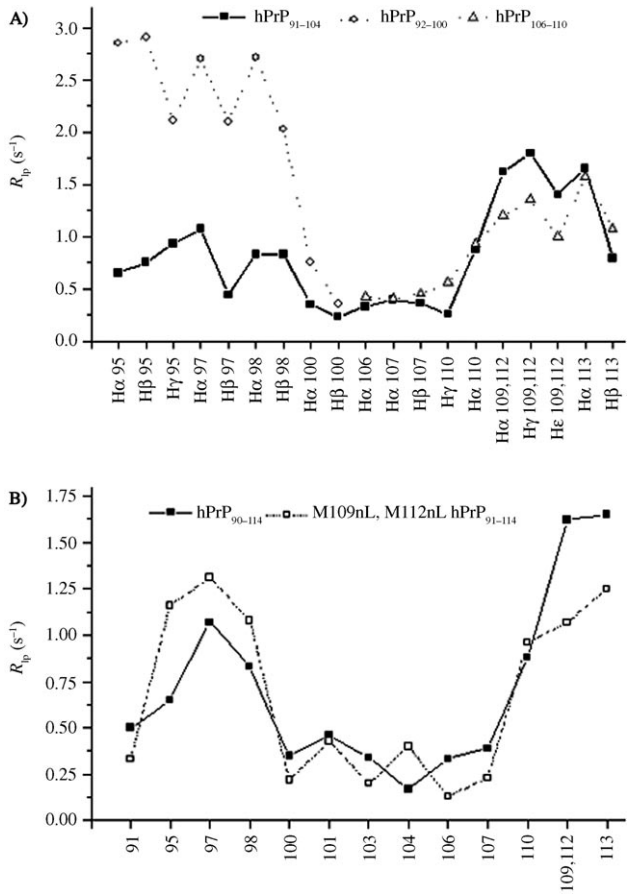

Figure 3. Comparison between the R_{1p} values of the LP2 fragment and those of: A) SP1 and SP2 and B) Met109→nLeu,Met112→nLeu LP2 analogue (only alpha protons are considered). All the values were calculated in the presence of 0.1 Cu^{II} equivalents.

ular dynamics simulations for obtaining a three-dimensional structure. In fact, R_{1p} is defined by Equation (1), where f and b refer to the free and metal-bound states, respectively, p is a fractional population of the peptide, R_{1f} and R_{1b} are the spin-lattice relaxation rates in the two environments, and k_{off}^{-1} (the inverse of the off-rate kinetic constant) is the residence time of the peptide in the metal coordination sphere.[49]

$$R_{1p} = R_{1obs} - p_f R_{1f} = \frac{p_b}{R_{1b}^{-1} + k_{off}^{-1}} \quad (1)$$

R_{1b} is the structure-sensitive term as accounted for by the Solomon equation describing the dipole–dipole nuclear-spin–electron-spin interaction.[50] The evaluation of the contribution of the exchange residence time allows the R_{1b} value to be obtained from measured R_{1p} values and the knowledge of the motional correlation time allows distances from the metal ion to be calculated by using the Solomon equation. In all calculations, values of $\tau_c=0.5$ ns for SP1 and $\tau_c=0.6$ ns for SP2 were used, as calculated from the Stokes equation applied to the free peptides in solution.

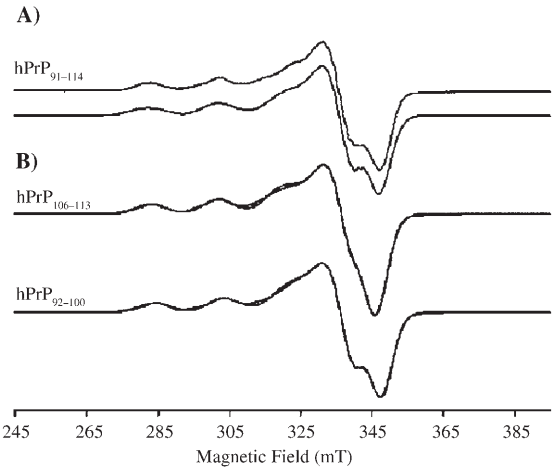

Figure 4. A) X-band EPR spectrum of the LP2 copper complex paired with the linear combination of experimental EPR spectra of the SP2 and SP1 copper complexes (15 and 85%, respectively). B) EPR spectra of SP2 and SP1 copper complexes paired with the simulations that gave the best fit (parameters reported in Table 2). $n=9.670$ GHz, modulation frequency = 100 KHz, modulation amplitude = 0.5 mT. All experiments were done with 4.5 mM peptide in the presence of 0.4 Cu^{II} equivalents at pH 6.5.

Table 2. EPR parameters for the 4.5 mM Cu^{II}–SP1 and Cu^{II}–SP2 complexes in presence of 0.4 Cu^{II} equivalents at pH 6.5

	$g_{\perp}$ [a]	$g_{\parallel}$	$A_{\perp}$ [b] [mT]	$A_{\parallel}$ [mT]	A^{N}_{iso} [mT]
SP1	2.06	2.22	0.6	18.9	1.40
SP2	2.05	2.23	1.5	18.0	1.45

[a] Error in g values is ±0.005. [b] Error in A values is ±0.2 mT.

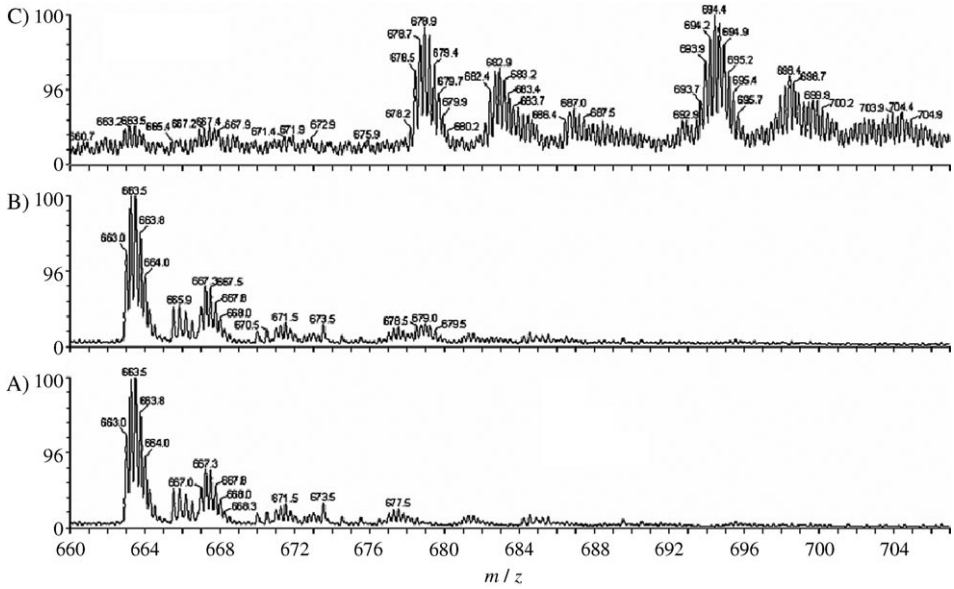

Figure 5. ESI mass spectra of A) 164 μM LP2 and after the addition of B) 0.4 and C) 1.25 Cu^{II} equivalents at pH 6.8.

As stated and applied elsewhere,[51] the R_{1p} value measured for the His Hε proton can be immediately considered for evaluating k_{off}^{im}, the off-rate for the imidazole ring from the metal coordination sphere, since the Hε proton is at a fixed distance (0.31 nm) from the paramagnetic center. The exchange rates calculated in this way at different peptide:-metal ratios are reported in Table 3 and they can immediately be used for ascertaining which imidazole nitrogen atom is bound to Cu^{II}, since the Cu^{II}–His-Hδ distance depends on Cu^{II} binding at the Nδ ($r=0.50$ nm) or at Nε atoms ($r=0.31$ nm).[51] It follows that both SP1 and SP2 coordinate the paramagnetic ion through the Nδ atom. The involvement of the same imidazolic nitrogen atom was reported for Ni^{II} complexes formed at high pH values with prion fragments containing either His96 or His111.[40]

Table 3. Paramagnetic relaxation contributions, R_{1p} [s^{-1}], exchange rate values, k_{off} [ms^{-1}], and copper distances, r [nm], for imidazole protons of the Cu^{II}–SP2 and Cu^{II}–SP1 complexes at $T=298$ K.

	+0.05 Cu^{II} equiv			+0.1 Cu^{II} equiv			+0.2 Cu^{II} equiv		
SP2									
	R_{1p}	r	k_{off}	R_{1p}	r	k_{off}	R_{1p}	r	k_{off}
Hε His	19	0.31	0.38	31	0.31	0.32	52	0.31	0.27
Hδ His	14	0.46		24	0.46		39	0.47	
SP1									
	R_{1p}	r	k_{off}	R_{1p}	r	k_{off}	R_{1p}	r	k_{off}
Hε His	68	0.31	1.6	n.d.[a]			n.d.[a]		
Hδ His	32	0.45		n.d.[a]			n.d.[a]		

[a] The resonances are so broad that measurement of the relaxation rates is prevented.

The exchange rate calculated for the imidazole ring is not likely to apply to backbone protons since binding is expected to occur as a multistep process that starts with the entrance of the anchoring site into the metal coordination sphere.[45,46,52] An estimate of the k_{off}^{bb} (backbone) value could be obtained by considering that binding to deprotonated amide nitrogen atoms belonging to a "X" generic residue (either towards the N- or C- terminal part) results in a Cu^{II}–Hα distance for the residue "X" ranging from 0.25–0.40 nm. The theoretical values of R_{1b} consistent with these distances were therefore calculated from the Solomon equation and inserted into Equation (1) to obtain k_{off}^{bb} values in the range of 54–61 s^{-1} for SP1 and 15–16 s^{-1} for SP2; these are, as expected, somehow slower than those calculated for the imidazole anchoring site.

The two limit values of k_{off}^{bb} allowed us to determine two different R_{1b} values for the remaining protons which yielded very similar metal–proton distances (Table 1), consistent with the r^6 dependence of the R_{1b} value that minimizes the error for relatively distant protons. As expected, the obtained results show that the slower the paramagnetic contribution (R_{1b}), the smaller the errors in the calculated distances.

The Cu^{II}-binding site centered at His96: As for Cu^{II}–SP1, the NMR results (Figure 4S in the Supporting Information and Figure 1 A) clearly identify His96 as the Cu^{II}-anchoring site but do not allow the unequivocal assignment of the two nitrogen donor atoms present in the metal coordination sphere: residues preceding as well as following His96 are similarly affected, such that the contemporaneous formation of two 3N copper complexes, both involving the His96 imidazole nitrogen atom but having diverse deprotonated amide nitrogen donors, can be suggested.

The calculated copper–proton distances (Table 1) and the direct Nδ–Cu^{II} bond were used as the only restraints in the molecular modeling of Cu^{II}–SP1; the simulated annealing protocol was applied to yield the structures of the metal complex.

The obtained structures of Cu^{II}–SP1 (Figure 6) show that the NMR restraints are consistent with two different but equally probable Cu^{II}-binding modes: the paramagnetic ion

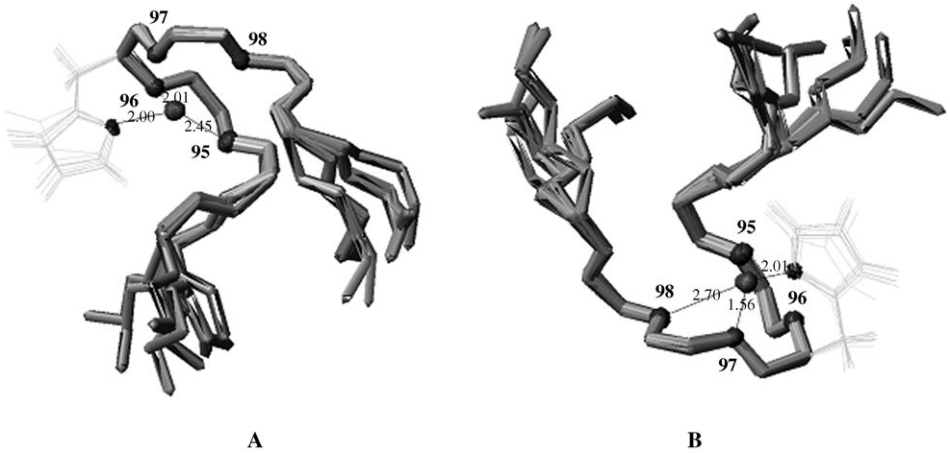

Figure 6. Superimposition of the first ten structures of the Cu^{II}–SP1 complex obtained from the DYANA simulation. The root mean square deviation (RMSD) value (taken on residues 94–98) is (0.10 ± 0.04) Å for the backbone atoms and (0.39 ± 0.14) Å for the heavy atoms. The figure was created with MOLMOL 2K.1.0. The two binding region are shown. A) The distances from the Thr95 and His96 amide nitrogen atoms and the His96 imidazole nitrogen atom to Cu^{II} are reported. B) The distances from the Ser97 and Gln98 amide nitrogen atoms and the His96 imidazole nitrogen atom to Cu^{II} are reported.

is bound to the His96 imidazole nitrogen atom and to either 1) the His96 and Thr95 deprotonated amide nitrogen atoms which are respectively 0.20 and 0.25 nm apart (Figure 6A) or 2) the Ser97 and Gln98 deprotonated amide nitrogen atoms which are respectively 0.20 and 0.28 nm apart (Figure 6B).

Generally, deprotonation and coordination of amide nitrogen atoms occurs in the N-terminal direction[53] because of the formation of a more favored six-membered $\{N_{imid},N^-\}$ chelate ring. However, the coexistence of a species involving residues in the opposite direction (Ser97 and Gln98), although yielding the less favored seven-membered $\{N_{imid},N^-\}$ chelate ring, is somehow stabilized by electrostatic interactions between the metal ion and the functional groups of the Gln98 and Trp99 side chains; moreover, consideration of the R_{1p} values reported in Table 1 shows that the Trp99 aromatic protons are among the most affected ones. This is consistent with the Trp99 indole ring approaching the metal ion closer than the Gln98 side chains (Figure 7) and providing a solvent-shielding hydrophobic environment that enhances the stability of the association. The occurrence of amide deprotonation towards the C terminus has never been proposed previously: EPR and CD data on peptide fragments encompassing His96 indicate the formation of stable 3N Cu^{II} complexes[37,39] and the coordination of amide nitrogen atoms in the N-terminal direction was suggested.

To support the coexistence of the two binding modes, a comparison was made between the binding abilities of two peptides: Ac-Gly-Gly-His,[54] in which Cu^{II} may coordinate amide nitrogens only toward the N terminus after anchoring at the His residue, and prion octarepeat Ac-Pro-His-Gly-Gly-Gly-Trp-Gly-Gln-NH_2[55] which coordinates towards the C terminus. The competition plot clearly indicates that 1) both ligands bind with the same affinity and 2) above pH 6, coordination towards the C terminus may be even more effective than that towards the N terminus (Figure 7S in the Supporting Information). Thus, alternative binding is very likely and it strongly depends on the side chains of the residues vicinal to the metal-ion-binding site.

The Cu^{II}-binding site centered at His111: In the case of Cu^{II}–SP2, the selective effects monitored on His111, Met112, and Ala113, shown in Figures 1A and 2, indicate that Cu^{II} anchoring at His111 is followed by deprotonation of amide nitrogen atoms towards the C terminus of the peptide.

Such coordination is likely to be stabilized by the Met side chain through hydrophobic protection resulting from electrostatic interaction of the sulfur atom with a metal-bound water molecule. As a matter of fact, energy minimization of the structures obtained from paramagnetic constraints, followed by a molecular dynamics simulation, determines a considerable approach of the Met112 side chain towards the metal, up to a distance of 0.34 nm (Figure 7). The absence of significant effects on the ε and γ Met resonances in the ^{13}C NMR spectra (Figure 2C), the measured Met Hε and Hγ R_{1p} values (Table 1), and all other spectroscopic measurements exclude the formation of a direct Cu–S bond, in disagreement with what has been recently reported for the Cu^{II}–hPrP106–114 complex.[42]

In a previous report,[46] the formation of a macrochelate involving the terminal NH_2 group and the His111 amide and imidazolic nitrogen atoms was suggested. The availability of the N-terminal group makes the investigated model completely different from other ones and forces copper coordination towards the N terminus. Moreover, previous potentiometric and spectroscopic studies performed on Cu^{II}–hPrP106–113[41] and Cu^{II}–hPrP106–114[42] were found to be consistent with a dominant 3N complex at physiological pH values, with two deprotonated amide nitrogen atoms bound to the metal. From the His111 anchoring site, the most logical (and thus suggested) coordination direction was towards the N terminus, but there was no direct evidence. On the other hand, Figure 2B shows that the most affected carbonyl resonances of SP2, upon Cu^{II} addition, are those of His111 and Met112, while almost no effects were monitored on the Met109 and Lys110 resonances; this indicates that the latter residues were at greater distances from the paramagnetic ion. Therefore, the broadening effects detected for the His111 and Met112 carbonyl groups might be considered as strong evidence for the direct involvement of the Met112 and Ala113 amide nitrogen atoms in metal binding.

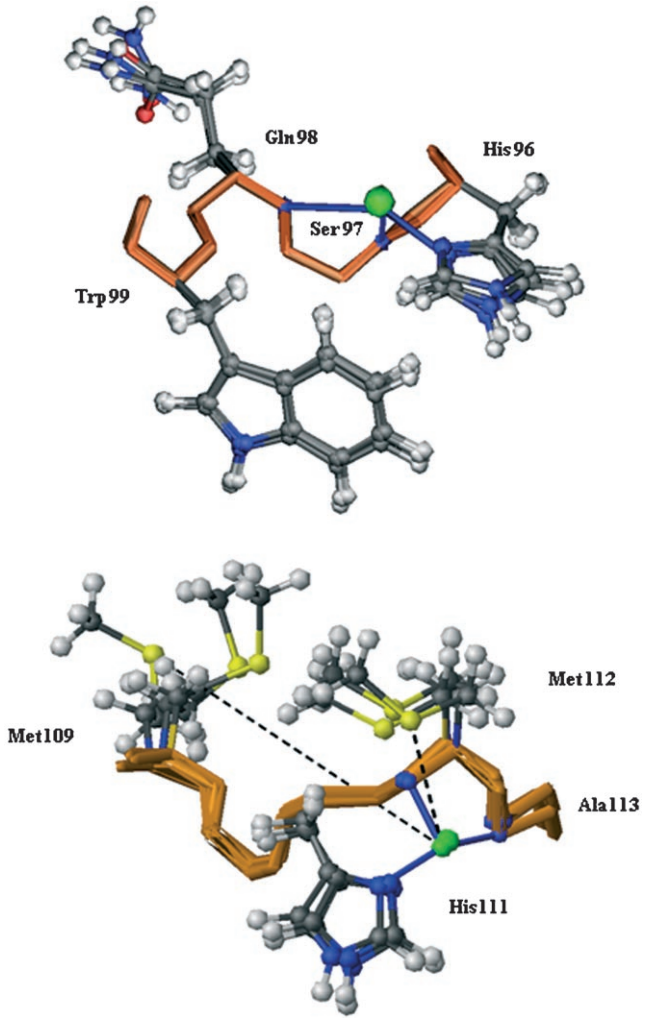

Figure 7. Top) Superimposition of the first four structures of the Cu^{II}–SP1 complex obtained from the DYANA simulation. The RMSD value (taken on residues 96–99) is (0.05 ± 0.03) Å for the backbone atoms and (0.34 ± 020) Å for the heavy atoms. Cu^{II} (green) is bound to the Ser97 and Gln98 amide nitrogen atoms and the His96 imidazole nitrogen atom. The Gln98 and Trp99 side chains are shown. Bottom) Cu^{II}–SP2 structure obtained from 25 ps molecular dynamics calculations showing the Cu^{II}–SMet distances (dotted lines): Cu^{II}–S (Met112) is 0.34 nm and Cu^{II}–S (Met109) is 1.1 nm. The figure was created with MOLMOL 2K.1.0.

Cu^{II}-binding affinities of the sites centered at His96 and His111: Finally, a comparison may be attempted of the affinities towards Cu^{II} of the binding sites provided by His96 in SP1 and by His111 in SP2. The obtained exchange rates, reported in Table 3, indicate a different copper affinity at the two His sites, with the His111 binding domain being three–four times stronger than the His96 one. This conclusion is also supported by the competition diagram shown in Figure 8, where the "binding abilities" of the peptides are compared. In the presence of equimolar amounts of copper and of the two ligands, SP2 is able to bind more metal ions (60%, approximately) than SP1.

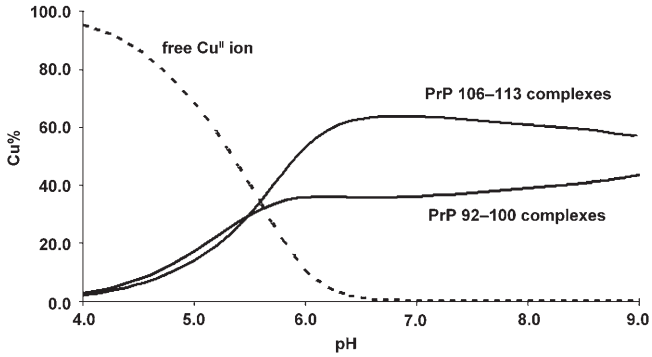

Figure 8. Competition plot between Cu^{II}–SP2 and Cu^{II}–SP1 complexes.

Cu^{II} binding in peptides encompassing both His96 and His111: The present EPR and NMR spectroscopy data, as well as previous EPR[37] and CD studies,[40] strongly suggest that the Cu^{II}-binding sites observed in SP1 and SP2 are preserved in peptides encompassing the whole region containing both His96 and His111 (LP1 or LP2). These latter peptides, in fact, bind Cu^{II} at one or the other of the His sites, at least as long as the concentration of peptide exceeds that of Cu^{II}. Such a conclusion is strongly supported by the potentiometric titrations performed for the 1:1 molar ratios clearly demonstrating the predominance of the equimolar complexes (Figure 2S and 3S in the Supporting Information) and it is definitively verified by the ESI mass spectra indicating the presence of 1:1 Cu^{II}–LP1 species only. ESI-MS experiments also demonstrate the coexistence of the two binding sites in the peptide with two Cu^{II} ions bound when Cu^{II} is in excess. Thus, the EPR, CD and NMR spectroscopy data collected for Cu^{II}–LP1 or Cu^{II}–LP2 should be, and they are, reproduced by linear combination of the same data collected for Cu^{II}–SP1 and Cu^{II}–SP2.

As a matter of fact, the 120 K EPR spectra of Cu^{II} bound by SP1, SP2, and LP1 (taken at the same ligand:Cu^{II} ratio) are very similar to each other and all are consistent with an almost tetragonal coordination sphere around Cu^{II} made by one oxygen and three nitrogen atoms. The linear combination that most satisfactorily reproduces the EPR spectrum of Cu^{II}–LP1 is made by approximately 85% of the EPR spectrum for Cu^{II}–SP1 and approximately 15% of that for Cu^{II}–SP2. These findings might be taken to suggest that the site located at His96 has a stronger binding affinity for Cu^{II} than the site located at His111, but this is in disagreement with the present NMR spectroscopy data and previous CD experiments,[40] where the linear combination that most precisely reproduces the CD spectra of Cu^{II}–hPrP91–115 is made up from approximately 72% of the His111 site and approximately 28% from the His96 site.[40]

The NMR spectra of Cu^{II}–LP1 (or LP2), recorded at 600 MHz, do not contain separate signals for the His96 and His111 Hε protons. However, the measured Hε R_{1p} value (21 s^{-1}) is consistent with $k_{off}^{im} = 0.96\ ms^{-1}$, faster than that calculated for Cu^{II}–SP2 ($k_{off}^{im} = 0.32\ ms^{-1}$) but slower than that calculated for Cu^{II}–SP1 ($k_{off}^{im} = 1.6\ ms^{-1}$). While again

ratifying that the two binding sites delineated for the "short" fragments are maintained in the "long" peptide, these findings apparently suggest that the binding sites located at His111 and His96 are differently populated in LP1. In particular, Figure 3A suggests that the binding site located at His96 is much less occupied than that located at His111. In fact, in the presence of 0.1 Cu^{II} equivalents, residues in the proximity of His96 in LP1 display R_{1p} values about three times smaller than those of the same residues in SP1. In order to evaluate the contributions of the two complexes, the k_{off}^{bb} rates calculated for Cu^{II}–SP2 ($k_{off}^{bb} = 16\ s^{-1}$) and for Cu^{II}–SP1 ($k_{off}^{bb} = 57\ s^{-1}$) were hypothesized to hold also in Cu^{II} complexes with LP1. These values were inserted in Equation (1) and the corresponding molar fractions (p_b) were calculated from the R_{1p} values: $p_b = 0.08$ and $p_b = 0.02$ were found for Cu^{II}–SP2 and Cu^{II}–SP1, respectively, thereby indicating that the binding site located at His111 gives a larger contribution (80%) than that located at His96 (20%). This result is in disagreement with the low-temperature EPR spectroscopy data but is consistent with SP2 displaying a stronger affinity than SP1 and agrees with the reported CD experiments at room temperature.[40]

Unfortunately, the coexistence of Cu^{II} complexes where the metal ion is bound at different sites prevents the determination of copper–proton distances from the measured R_{1p} value, which is a value averaged over the two available copper-binding sites. However, the molecular dynamics calculations performed at variable temperatures on Cu^{II}–SP2 may provide a valuable clue for explaining the disagreement between the low-temperature EPR spectroscopy data and the room-temperature CD and NMR spectroscopy data. The calculations show that at 120 K the Met112 side chain is relatively far from Cu^{II}, such that no stabilization of the binding site located at His111 can be provided. The Cu^{II}–S (Met112) distance, monitored every ps along the whole MD trajectory (Figure 9), levels off at 0.54 nm. At this temperature, the fact that binding at His96 can offer two different ways of coordination may result in a larger statistical weight for this site over that provided by His111. At 300 K, the Met112 side chain approaches the metal, with the Cu^{II}–S distance ranging from 0.30–0.40 nm during the MD trajectory (Figure 9). The stabilization provided by the Met hydrophobic side chain approaching the metal may explain why the site located at His111 becomes much more populated than the other one at room temperature.

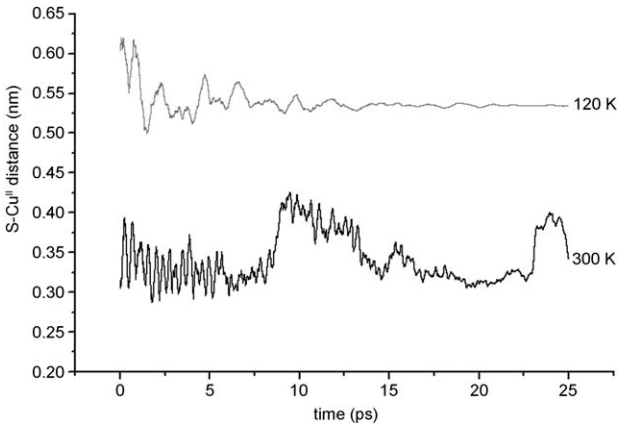

Figure 9. Cu^{II}–S (Met112) distances monitored during 25 ps MD simulation of the Cu^{II}–SP2 complex at $T = 120$ K (gray line) and $T = 300$ K (black line).

In conclusion, the hPrP region immediately outside the octarepeat region offers two independent Cu^{II}-binding sites. In both, Cu^{II} first anchors at the imidazole nitrogen atom and successively deprotonates, at pH 6.5, two amide nitrogen atoms. The hydrophobic protection furnished by the Met112 side chain makes the binding site centered at His111 two–threefold stronger than that centered at His96 at room temperature. This stronger affinity does not in any way prevent entrance of Cu^{II} to the other site, so that more than one species simultaneously exists in solution and the species are in fast exchange with each other. Comparison with shorter fragments demonstrates that the structures of the binding modes are maintained.

Experimental Section

Details of the methods used to synthesize, purify, and characterize the investigated peptides are given in the Supporting Information.

Potentiometric measurements: Stability constants both for proton and Cu^{II} complexes were calculated from 3 or 4 titrations carried out over the range pH 3–11 at 25°C with a total volume of 1.5 mL. The purities and exact concentrations of the solutions of ligands were determined by the Gran method.[56] NaOH was added from a 0.250-mL micrometer syringe, which was calibrated by both weight titration and the titration of standard materials. The metal-ion concentration was 1×10^{-3} M and the metal/ligand ratio was 1:1. The pH-metric titrations were performed at 25°C in 0.1 M KCl on a MOLSPIN pH-meter system with a Russel CMAW 711 semicombined electrode calibrated in hydrogen concentrations by using standard HCl[57] or on an Orion EA 940 pH meter (resolution 0.1 mV, accuracy 0.2 mV) equipped with a combined glass electrode (Metrohm EA125) and a Hamilton MicroLab M motor burette (resolution 0.1 μL, accuracy 0.2 μL) equipped with a Hamilton syringe (delivery volume 250 μL). Constant-speed magnetic stirring was applied throughout. The temperature of the titration cell was kept at 298.2 K by use of a Haake F3C circulation thermostat. UPP grade nitrogen, previously saturated with H_2O (0.1 M KNO_3, 298.2 K), was blown over the test solution in order to maintain an inert atmosphere. The SUPERQUAD program was used for stability-constant calculations.[58] Standard deviations were computed by SUPERQUAD and refer to random errors only. They are, however, a good indication of the importance of a particular species in the equilibrium.

CD measurements: Solutions were of similar concentrations to those used in the potentiometric studies. Absorption spectra were recorded either on a Beckman DU 650 or a Cary 50 (Varian) spectrophotometer, at room temperature. CD spectra were recorded on a Jasco J-715 spectropolarimeter in the 800–235 nm range.

NMR spectroscopy: The peptides were dissolved in water containing 10% deuterium oxide (^{1}H NMR) or in deuterium oxide (^{13}C NMR). Solutions were carefully deoxygenated. The pH value was adjusted with either DCl or NaOD. The desired concentrations of metal ions were obtained by adding aliquots of stock water solutions of $Cu(NO_3)_2$, and the pH value was again checked and eventually readjusted. NMR experiments were carried out at 14.1 T at a controlled temperature (±0.1 K) on a Bruker Avance 600 MHz spectrometer equipped with a Silicon Graphics workstation. Suppression of the residual water signal was achieved either by presaturation or by excitation sculpting,[59] by using a selective

square pulse for 2 ms on water. Proton resonance assignments were obtained by COSY, TOCSY, NOESY, and ROESY experiments. Carbon resonance assignments were obtained by HSQC and HMBC experiments carried out with standard pulse sequences. $^{1}H–^{13}C$ HSQC alpha cross-peaks affected during Cu^{II} titration were identified by comparing their intensities (I) with those of the same cross-peaks (I_0) observed in the absence of the paramagnetic ion. Proton spin-lattice relaxation rates ($R_1 = 1/T_1$) were measured with the standard inversion-recovery pulse sequence; relaxation rates were calculated with regression analysis of the initial recovery curves of the longitudinal magnetization components, a process leading to errors in the range $\pm 3\%$. While the simple inversion-recovery experiment is suitable for the well-isolated peaks, the IR-TOCSY sequence was used to calculate the relaxation rates of the overlapping ^{1}H NMR signals.[60] This was obtained by introducing a ^{1}H 180° pulse, followed by a variable delay in front of the TOCSY sequence. The T_1 values were determined by a three-parameter fit of the peak intensities to Equation (2), where B is variable parameter that considers nonideal magnetization and which has a value smaller than one.

$$I(\tau(= I_0[1-(1+B)\exp(-\tau/T_1)] \quad (2)$$

The obtained results were compared with those obtained from the normal IR sequence. Agreement was found within the error limits of both experiments.

EPR spectroscopy: EPR spectroscopy experiments were performed on solutions of similar concentrations to those used for the NMR spectroscopy studies. CW-X-band (9.4 GHz) EPR measurements were carried out with a Bruker E500 Elexsys series instrument by using a Bruker ER 4122 SHQE cavity and a Bruker ER 4111 VT temperature-control apparatus. The EPR spectra were simulated by using a simulation program for rigid motion included in the COSMOS package which is based on a general theory for the calculation of conventional CW-EPR spectra under virtually all motional conditions.[61]

Electron-spray-ionization mass spectrometry (ESI-MS): ESI-MS data were collected on a Q-TOF microTM (Micromass, Waters Corporation, Milford, MA) mass spectrometer. Peptides were dissolved in Milli-Q water (164 mM) with the pH value adjusted by adding diluted NaOH solution. The metal-complex samples were prepared by adding $Cu(NO_3)_2$ in Milli-Q water (1.2 mM) at ligand:Cu^{II} ratios of 1:1.25 and 1:0.4. The pH values were comparable after the addition of Cu^{II}. Sample solutions were injected into the spectrometer system at a flow rate of 5 $\mu L\,min^{-1}$. Spectra were acquired in positive-ion mode by applying the following experimental conditions: capillary voltage 3.0 kV; cone potential 30 V; source temperature 150 °C. For the recording of mass spectra, TOF data were acquired by accumulation of 10 multiple channel acquisition (MCA) scans over mass ranges of m/z 300–3000.Data acquisition was optimized to supply the highest possible resolution and the best signal-to-noise ratio, even in the case of low-abundance signals. To simplify the peak assignments, the fragment annotations indicated in the text and in the figures correspond to the lowest mass peak of each isotopic cluster.

Molecular dynamics: All R_{1p} values, obtained from NMR measurements, were converted into distance constraints and used to build a pseudo potential energy for a molecular dynamics calculation. In this procedure, the potential energy is a function of the difference between the distance constraints provided by the user and the corresponding distances found in a given conformer (target function). No other potential energy terms are present except the van der Waals repulsion. At the beginning of the calculation an arbitrary number of different conformers is generated by randomly varying torsional dihedral angles. The potential energy is then minimized by a simulated annealing procedure in the torsion angle space, in which the system is brought to high temperature to allow all possible high-energy starting conformations and subsequently cooled down in order to stabilize it in those potential energy minima that best satisfy the imposed constraints. In particular, we performed the calculation with the program DYANA,[62] by using 10000 steps and 300 random relative starting positions of the peptides and Cu^{II}. The obtained structures were then optimized through an energy minimization followed by a 30 ps restrained molecular dynamics simulation at two different temperature values, 120 and 300 K (5 ps to bring the system to the desidered temperature, followed by 25 ps at a constant temperature), by using the program Hyperchem[63] with the MM^{+} force field.

Acknowledgements

This work was partly supported by the Polish Ministry of Education and Science (grant nos.: MEIN 1T09 A00830 and DS/8290-4-0129-4). Some of the 600 MHz $^{1}H–^{13}C$ HSQC spectra were recorded at the UNIFRA Large Scale Facility in Frankfurt; the support of the European Community (Access to Research Infrastructure action of the Improving Human Potential Program) is gratefully acknowledged.

[1] D. R. Brown, B. S. Wong, F. Hafiz, C. Clive, S. Haswell, I. M. Jones, *Biochem. J.* **1999**, *344*, 1–5.
[2] S. B. Prusiner, *Proc. Natl. Acad. Sci. USA* **1998**, *95*, 13363–13383.
[3] A. M. Thackray, R. Knight, S. J. Haswell, R. Bujdoso, D. R. Brown, *Biochem. J.* **2002**, *362*, 253–258.
[4] E. Gaggelli, H. Kozlowski, D. Valensin, G. Valensin, *Chem. Rev.* **2006**, *106*, 1995–2044.
[5] K. M. Pan, M. Baldwin, J. Nguyen, M. Gasset, A. Serban, D. Groth, I. Melhorn, Z. Huang, R. J. Fletterick, F. E. Cohen, S. B. Prusiner, *Proc. Natl. Acad. Sci. USA* **1993**, *90*, 10962–10966.
[6] D. C. Bolton, M. P. McKinley, S. B. Prusiner, *Science* **1982**, *218*, 1309–1311.
[7] M. P. McKinley, D. C. Bolton, S. B. Prusiner, *Cell* **1983**, *35*, 57–62.
[8] S. J. De Armond, M. P. McKinley, A. Barry, M. B. Braunfeld, J. R. McColloch, S. B. Prusiner, *Cell* **1985**, *41*, 221–235.
[9] B. Caughey, G. J. Raymond, *J. Biol. Chem.* **1991**, *266*, 18217–18223.
[10] N. Stahl, A. Baldwin, D. B. Teplow, L. Hood, B. W. Gibson, A. L. Burlingame, S. B. Prusiner, *Biochemistry* **1993**, *32*, 1991–2002.
[11] D. A. Lysek, C. Schorn, L. G. Nivon, V. Esteve-Moya, B. Christen, L. Calzolai, C. Von Schroetter, F. Fiorito, T. Herrmann, P. Guntert, K. Wuthrich, *Proc. Natl. Acad. Sci. USA* **2005**, *102*, 640–645.
[12] L. Calzolai, D. A. Lysek, D. R. Perez, P. Guntert, K. Wuthrich, *Proc. Natl. Acad. Sci. USA* **2005**, *102*, 651–655.
[13] A. D. Gossert, S. Bonjour, D. A. Lysek, F. Fiorito, K. Wuthrich, *Proc. Natl. Acad. Sci. USA* **2005**, *102*, 646–650.
[14] R. Zahn, A. Liu, T. Luhrs, R. Riek, C. von Schroetter, F. Lopez Garcia, M. Billeter, L. Calzolai, G. Wider, K. Wuthrich, *Proc. Natl. Acad. Sci. USA* **2000**, *97*, 145–150.
[15] A. L. Horwich, J. S. Weissman, *Cell* **1997**, *89*, 499–510.
[16] D. R. Brown, K. Qin, J. W. Herms, A. Madlung, J. Manson, R. Strome, P. E. Fraser, T. A. Kruck, A. von Bohlen, W. Schulz-Schaeffer, A. Giese, D. Westaway, H. Kretzschmar, *Nature* **1997**, *390*, 684–687.
[17] D. R. Brown, F. Hafiz, L. L. Glassmith, B. S. Wong, I. M. Jones, C. Clive, S. J. Haswell, *EMBO J.* **2000**, *19*, 1180–1186.
[18] G. S. Jackson, I. Murray, L. L. P. Hosszu, N. Gibbs, J. P. Waltho, A. R. Clarke, J. Collinge, *Proc. Natl. Acad. Sci. USA* **2001**, *98*, 8531–8535.
[19] S. Lehmann, *Curr. Opin. Chem. Biol.* **2002**, *6*, 187–192.
[20] D. R. Brown, H. Kozlowski, *Dalton Trans.* **2004**, 1907–1917.
[21] G. L. Millhauser, *Acc. Chem. Res.* **2004**, *37*, 79–85.
[22] J. H. Viles, F. E. Cohen, S. B. Prusiner, D. B. Goodin, P. E. Wright, J. H. Dyson, *Proc. Natl. Acad. Sci. USA* **1999**, *96*, 2042–2047.
[23] A. P. Garnett, J. H. Viles, *J. Biol. Chem.* **2003**, *278*, 6795–6802.
[24] C. S. Burns, E. Aronoff-Spencer, C. M. Dunham, P. Lario, N. I. Avdievich, W. E. Antholine, M. M. Olmstead, A. Vrielink, G. J. Gerfen, J. Peisach, W. G. Scott, G. L. Milhauser, *Biochemistry* **2002**, *41*, 3991–4000.
[25] D. Valensin, M. Łuczkowski, F. M. Mancini, A. Łęgowska, E. Gaggeli, G. Valensin, K. Rolka, H. Kozłowski, *Dalton Trans.* **2004**, 1284–1293.

[26] E. Flechsig, D. Shmerling, I. Hegyi, A. J. Raeber, M. Fischer, A. Cozzio, C. von Mering, A. Aguzzi, C. Weissmann, *Neuron* **2000**, *27*, 399–408.
[27] M. L. Kramer, H. D. Kratzin, B. Schmidt, A. Römer, O. Windl, S. Liemann, S. Hornemann, H. Kretzschmar, *J. Biol. Chem.* **2001**, *276*, 16711–16719.
[28] A. R. Thompsett, S. R. Abdelraheim, M. Daniels, D. R. Brown, *J. Biol. Chem.* **2005**, *280*, 42750–42758.
[29] M. F. Jobling, X. Huang, L. R. Stewart, K. J. Barnham, C. Curtain, I. Volitakis, M. Perugini, A. R. White, R. A. Cherny, C. L. Masters, C. J. Barrow, S. J. Collins, A. I. Bush, R. Cappai, *Biochemistry* **2001**, *40*, 8073–8084.
[30] G. M. Cereghetti, A. Schweiger, R. Glockshuber, S. Van Doorslaer, *Biophys. J.* **2001**, *81*, 516–525.
[31] T. Muramoto, M. Scott, F. E. Cohen, S. B. Prusiner, *Proc. Natl. Acad. Sci. USA* **1996**, *93*, 15457–15462.
[32] F. Tagliavini, F. Prelli, L. Verga, G. Giaccone, R. Sarma, P. Gorevic, B. Betti, F. Passerini, E. Ghibaudi, G. Forloni, M. Solmona, O. Bugiani, B. Frangione, *Proc. Natl. Acad. Sci. USA* **1993**, *90*, 9678–9682.
[33] M. Fischer, T. Rulicke, A. Raeber, A. Sailer, M. Moser, B. Oesch, S. Brandner, A. Aguzzi, C. Weissmann, *EMBO J.* **1996**, *15*, 1255–1264.
[34] T. Muramoto, S. J. DeArmond, M. Scott, G. C. Telling, F. E. Cohen, S. B. Prusiner, *Nat. Med.* **1997**, *3*, 750–755.
[35] D. R. Brown, B. Schmidt, H. A. Kretzschmar, *Nature* **1996**, *380*, 345–347.
[36] S. R. Abdelraheim, S. Královicová, D. R. Brown, *Int. J. Biochem. Cell Biol.* **2006**, *38*, 1429–1440.
[37] C. S. Burns, E. Aronoff-Spencer, G. Legname, S. B. Prusiner, W. E. Antholine, G. J. Gerfen, J. Peisach, G. L. Millhauser, *Biochemistry* **2003**, *42*, 6794–6803.
[38] S. S. Hasnain, L. M. Murphy, R. W. Strange, J. G. Grossmann, A. R. Clarke, G. S. Jackson, J. Collinge, *J Mol. Biol.* **2001**, *311*, 467–473.
[39] C. E. Jones, S. R. Abdelraheim, D. R. Brown, J. H. Viles, *J. Biol. Chem.* **2004**, *279*, 32018–32027.
[40] C. E. Jones, M. Klewpatinond, S. R. Abdelraheim, D. R. Brown, J. H. Viles, *J. Mol. Biol.* **2005**, *346*, 1393–1407.
[41] M. Remelli, M. Donatoni, R. Guerrini, A. Janicka, P. Pretegiani, H. Kozlowski, *Dalton Trans.* **2005**, *17*, 2876–2885.
[42] G. Di Natale, G. Grasso, G. Impellizzeri, D. La Mendola, G. Micera, N. Mihala, Z. Nagy, K. Osz, G. Pappalardo, V. Rigo, E. Rizzarelli, D. Sanna, I. Svago, *Inorg. Chem.* 2005, 44, 7214–7225.
[43] L. D. Petit, S. Pyburn, W. Bal, H. Kozłowski, M. Bataille, *J. Chem. Soc. Dalton Trans.* **1990**, 3565–3570.
[44] P. G. Daniele, E. Prenesti, G. Ostacolli, *J. Chem. Soc. Dalton Trans.* **1996**, 3269–3275.
[45] B. Belosi, E. Gaggelli, R. Guerrini, H. Kozłowski, M. Łuczkowski, F. M. Mancini, M. Remelli, D. Valensin, G. Valensin, *ChemBioChem* **2004**, *5*, 349–359.
[46] E. Gaggelli, F. Bernardi, E. Molteni, R. Pogni, D. Valensin, G. Valensin, M. Remelli, M. Luczkowski, H. Kozlowski, *J. Am. Chem. Soc.* **2005**, *127*, 996–1006.
[47] G. Della Lunga, R. Pogni, R. Basosi, *J. Magn. Reson. Ser. A* **1995**, *114*, 174–178.
[48] J. Peisach, W. E. Blumberg, *Arch. Biochem. Biophys.* **1974**, *165*, 691–708.
[49] I. Bertini, C. Luchinat, G. Parigi, *Curr. Methods Inorg. Chem.* **2001**, *2*, 1–372.
[50] I. Solomon, *Phys. Rev.* **1955**, *99*, 559–565.
[51] E. Gaggelli, H. Kozłowski, D. Valensin, G. Valensin, *Mol. BioSystems* **2005**, *1*, 79–84.
[52] P. Stańczak, D. Valensin, P. Juszczyk, Z. Grzonka, G. Valensin, F. Bernardi, E. Molteni, E. Gaggelli, H. Kozlowski, *Chem. Commun.* **2005**, *14*, 3298–3300.
[53] H. Kozłowski, W. Bal, M. Dyba, T. Kowalik-Jankowska, *Chem. Rev.* **1999**, *99*, 319–346.
[54] G. F. Bryce, R. W. Roesce, F. R. N. Gurd, *J. Biol. Chem.* **1966**, *241*, 1072–1080.
[55] M. Luczkowski, H. Kozlowski, M. Slawikowski, K. Rolka, E. Gaggelli, D. Valensin, G. Valensin, *J. Chem. Soc. Dalton Trans.* **2002**, 2269–2274.
[56] G. Gran, *Acta Chem. Scand.* **1950**, *4*, 559–577.
[57] H. Irving, M. G. Miles, L. D. Pettit, *Anal. Chim. Acta* **1967**, *38*, 475–488.
[58] P. Gans, A. Sabatini, A. Vacca, *J. Chem. Soc. Dalton Trans.* **1985**, 1195–1200.
[59] T. L. Hwang, A. J. Shaka, *J. Magn. Reson. Ser. A* **1995**, *112*, 275–279.
[60] J. G. Huber, J. M. Moulis, J. Gaillard, *Biochemistry* **1996**, *35*, 12705–12711.
[61] G. Della Lunga, M. Pezzato, M. C. Baratto, R. Pogni, R. Basosi, *J. Magn. Reson. Ser. A* **2003**, *164*, 71–77.
[62] P. Güntert, C. Mumenthaler, K. Wüthrich, *J. Mol. Biol.* **1997**, *273*, 283–298.
[63] HYPERCHEM, Hypercube release 5.1 Pro for Windows, Hypercube Inc., Waterloo, Canada, **1997**.

Received: August 24, 2006
Published online: December 7, 2006

